Local Dissipation Scales and Integral-Scale Reynolds Number Scalings in Thermally-Driven Turbulence

Journal of Physics: Conference Series **318** (2011) 042016 doi:10.1088/1742-6596/318/4/042016

Local Dissipation Scales and Integral-Scale Reynolds Number Scalings in Thermally-Driven Turbulence

Ke-Qing XIA[1], **Quan ZHOU**[2]

[1]Department of Physics, The Chinese University of Hong Kong, Shatin, Hong Kong, China
[2]Shanghai Key Laboratory of Mechanics in Energy and Environment Engineering, Shanghai Institute of Applied Mathematics and Mechanics, Shanghai University, Shanghai 200072, China

E-mail: kxia@phy.cuhk.edu.hk

Abstract. We present direct multi-point velocity measurements of the two-dimensional velocity fields in a cylindrical Rayleigh-Bénard convection cell using the particle image velocimetry (PIV) technique over the Rayleigh number range $5.9 \times 10^9 \lesssim Ra \lesssim 1.1 \times 10^{11}$. The longitudinal integral length scale of the horizontal and vertical velocity fields are obtained at the cell center, near the cell sidewall, and near the bottom plate of the cell, respectively. In addition, the Reynolds number based on these scales, Re_{Lx} and Re_{Lz}, are obtained. It is found that all measured Re_L scales as $Re_L \sim Ra^\beta$, with the exponent $\beta \simeq 0.5$, except Re_{Lx} for the horizontal velocity at the cell center, which has a $\beta \simeq 0.75$. The local dissipation scale field η at the three different places are also studied. Our results reveal two types of universality of η. The first one is that, for the same flow, the probability density functions (PDF) of η are insensitive to turbulent intensity and large-scale inhomogeneity and anisotropy of the system. The second is that the small-scale dissipation dynamics in buoyancy-driven turbulence can be described by the same models developed for homogeneous and isotropic turbulence. However, the exact functional form of the PDF of the local dissipation scale is not universal with respect to different types of flows, but depends on the integral-scale velocity boundary condition, which is found to have an exponential, not Gaussian, distribution in turbulent Rayleigh-Bénard convection.

1. Introduction

Fluid turbulence exhibits intermittent nature ubiquitously, such as intense spikes of velocity gradients and energy dissipation rates in both space and time. Such behaviors are usually studied quantitatively by investigating the cascades of turbulent kinetic energy transferred continuously from large to small scales (Frisch, 1995; Sreenivasan & Antonia, 1997; Ishihara *et al.*, 2009). In the classical Kolmogorov's theory (Kolmogorov, 1941), this cascade process would stop at the smallest length scale of turbulence, known as the Kolmogorov dissipation scale η_K, below which energy is dissipated into heat. Based on dimensional arguments, η_K can be derived as $\eta_K = (\nu^3/\langle\epsilon\rangle)^{1/4}$, where ν is the kinematic viscosity of the fluid. As a mean length obtained from the mean energy dissipation rate $\langle\epsilon\rangle$, however, η_K precludes the intermittent nature of turbulence. To establish a connection between the dissipation scale and the intensive and localized turbulent events, Paladin & Vulpiani (1987) put forward the idea of a local dissipation scale, i.e. the local Reynolds number associated with an eddy of length scale η is of order 1:

$$Re_\eta = \eta|\delta_\eta v|/\nu \sim 1. \quad (1)$$

Table 1. Experimental conditions and parameters for measurements performed at cell center. L_x and L_z are the longitudinal integral length scales, respectively, in the horizontal and vertical directions. Re_{Lx} and Re_{Lz} are Reynolds numbers based on L_x and L_z, respectively. The scales η_{0x} and η_{0z} are calculated as $\eta_{0x} = L_x \mathrm{Re}_{Lx}^{-0.72}$ and $\eta_{0z} = L_z \mathrm{Re}_{Lz}^{-0.72}$, and the averaged scale $\eta_0 = (\eta_{0x} + \eta_{0z})/2$. η_K is the global Kolmogorov scale.

No.	Ra	L_x (m)	L_z (m)	Re_{Lx}	Re_{Lz}	η_{0x} (mm)	η_{0z} (mm)	η_0 (mm)	η_K (mm)	Δ_l/η_0
1	5.9×10^9	0.091	0.066	219	136	1.77	1.83	1.80	1.30	0.33
2	1.1×10^{10}	0.103	0.070	379	217	1.34	1.37	1.36	1.07	0.44
3	2.9×10^{10}	0.111	0.069	717	367	0.91	0.93	0.92	0.79	0.64
4	5.7×10^{10}	0.130	0.062	1238	428	0.72	0.74	0.73	0.63	0.81
5	1.1×10^{11}	0.161	0.070	2068	709	0.61	0.58	0.59	0.51	1.00

Here, $\delta_\eta v = v_r(r+\eta) - v_r(r)$ is the longitudinal velocity increment over a separation η. Such a definition implies a local balance between the inertial force $(\delta_\eta v)^2/\eta$ and the viscous force $\nu|\delta_\eta v|/\eta^2$ at a particular point in space and time. The resulting η is therefore a field that fluctuates in both space and time and hence may be used to reflect intermittency. Recently, the probability density function (PDF) of η, $Q(\eta)$, within the range $0 < \eta < L$ (L is the integral length scale of the turbulence) was proposed analytically by Yakhot (2006, 2008) based on the Mellin transform of structure functions and by Biferale (2008) based on the multifractal formalism. Both analytical predictions consist of distributions of scales varying from very fine sub-Kolmogorov scales, related to the very intense velocity gradients in the form of slender vortex filaments with diameters of order η_K or even less, to those much larger than η_K. Results obtained later from high-resolution numerical simulations of homogeneous and isotropic box turbulence (Schumacher, 2007; Schumacher, Sreenivasan & Yakhot, 2007) and experiments in turbulent pipe flows (Bailey *et al.*, 2009) were both found to agree well with the theoretical distributions. These results seem to suggest a universality of the smallest-scale fluctuations around η_K, but further tests in different types of turbulent flows are needed.

In this paper we want to generalize these ideas into the thermally-driven turbulence, an important class of turbulent flows that plays an essential role in many natural processes. The flow at hand is turbulent convection in a fluid layer heated from below and cooled from above, i.e. turbulent Rayleigh-Bénard convection (RBC), which has become a paradigm for understanding the thermally-driven turbulence (Ahlers *et al.*, 2009; Lohse & Xia, 2010). Cascades of velocity and temperature fluctuations in such a system have been studied extensively in the past two decades (Lohse & Xia, 2010). Here, we report measurements of the integral-scale Reynolds number scaling and the local dissipation scale distribution at three representative locations in a cylindrical turbulent RBC cell. Some of the results concerning local-dissipation scale presented here have been previously reported elsewhere (Zhou & Xia, 2010), in the present paper we provide more experimental details and measured parameters. In addition, we report new results concerning the integral-scale Reynolds number scaling.

2. Experimental setup and parameters

Table 2. Experimental conditions and parameters for measurements performed near the cell sidewall.

No.	Ra	L_x (m)	L_z (m)	Re_{Lx}	Re_{Lz}	η_{0x} (mm)	η_{0z} (mm)	η_0 (mm)	η_K (mm)	Δ_l/η_0
1	5.9×10^9	0.031	0.151	58	568	1.59	1.47	1.53	1.30	0.39
2	1.1×10^{10}	0.031	0.145	87	816	1.19	1.08	1.14	1.07	0.52
3	2.0×10^{10}	0.033	0.149	117	945	1.03	1.00	1.02	0.88	0.58
4	2.9×10^{10}	0.034	0.147	147	1091	0.89	0.89	0.89	0.79	0.66
5	4.0×10^{10}	0.029	0.143	144	1340	0.77	0.75	0.76	0.71	0.78
6	5.7×10^{10}	0.033	0.156	196	1820	0.69	0.65	0.67	0.63	0.88
7	8.1×10^{10}	0.033	0.146	229	1946	0.62	0.58	0.60	0.56	0.99
8	9.5×10^{10}	0.031	0.134	258	2160	0.54	0.49	0.52	0.54	1.15
9	1.1×10^{11}	0.031	0.155	252	2577	0.54	0.50	0.52	0.51	1.14

Table 3. Experimental conditions and parameters for measurements performed near the bottom plate.

No.	Ra	L_x (m)	L_z (m)	Re_{Lx}	Re_{Lz}	η_{0x} (mm)	η_{0z} (mm)	η_0 (mm)	η_K (mm)	Δ_l/η_0
1	5.9×10^9	0.093	0.029	353	67	1.29	1.32	1.30	1.30	0.45
2	1.1×10^{10}	0.101	0.028	496	94	1.09	1.03	1.06	1.07	0.56
3	2.0×10^{10}	0.109	0.029	695	122	0.92	0.86	0.89	0.88	0.67
4	2.9×10^{10}	0.105	0.028	883	152	0.74	0.72	0.73	0.79	0.81
5	4.0×10^{10}	0.104	0.028	966	174	0.69	0.64	0.67	0.71	0.90
6	5.7×10^{10}	0.105	0.028	1098	206	0.63	0.57	0.60	0.63	0.99
7	8.1×10^{10}	0.103	0.028	1315	246	0.55	0.50	0.52	0.56	1.13
8	9.5×10^{10}	0.113	0.029	1599	273	0.52	0.48	0.50	0.54	1.18

The convection cell is similar to that used in previous experiments (Sun *et al.*, 2005), but has a different size (Zhou & Xia, 2010; Zhou *et al.*, 2011). Briefly it is a vertical cylinder with top and bottom copper plates and plexiglas sidewall, with its height H and inner diameter both being 50 cm. During the experiment the entire cell was wrapped by several layers of Styrofoam and the cell was tilted by a small angle of about 0.5° so that the measurements were carried out within the vertical plane of the large-scale circulation. The mean temperature of water was kept at 29°, corresponding to a Prandtl number $Pr = \nu/\kappa = 5.5$. The experiment covered the range $5.9 \times 10^9 \lesssim Ra \lesssim 1.1 \times 10^{11}$ of the Rayleigh number $Ra = \alpha g \Delta T H^3/\nu\kappa$, with g being the gravitational acceleration, ΔT the temperature difference across the fluid layer, and α and κ being, respectively, the thermal expansion coefficient and the thermal diffusivity of the working fluid (water). The velocity field was measured by the particle image velocimetry (PIV) technique with a measuring area of 3.7×3.7 cm^2 and a spatial resolution $\Delta_l = 0.59$ mm, corresponding to 63×63 measured velocity vectors. Hollow glass spheres of 10-μm-diameter were used as seed particles. The PIV measurements were performed at three different places of the cell: its center, 2 cm from the sidewall at mid-height, and 2 cm above the center of the bottom plate. Denote the laser-illuminated plane as the xz plane, the horizontal velocity component $u(x, z)$ and the vertical one $w(x, z)$ were then obtained. Each measurement lasted 3 hours in which a total of 25 000 two-dimensional vector maps were acquired with a sampling rate ~ 2.3 Hz. The

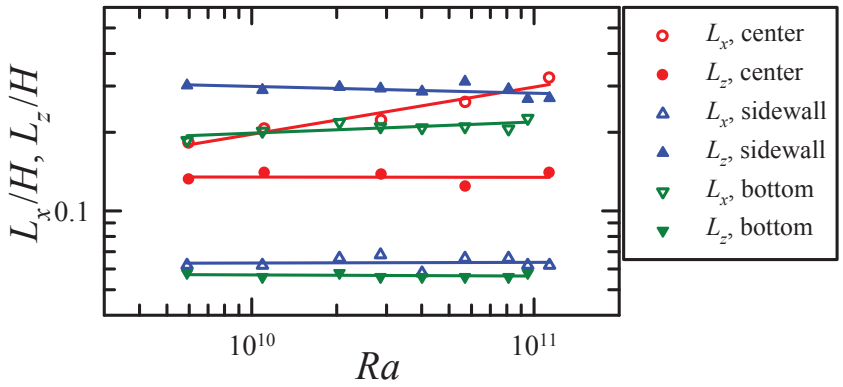

Figure 1. The Ra-dependence of L_x/H (open symbols) and L_z/H (sold symbols) measured at cell center (red circles), near the cell sidewall (blue up-triangles), and near the bottom plate (green down-triangles). The lines represent power-law fits to the data: $L_x/H \sim Ra^{0.18\pm0.05}$ and $L_z/H \sim Ra^{-0.0016\pm0.05}$ at the cell center, $L_x/H \sim Ra^{0.0028\pm0.04}$ and $L_z/H \sim Ra^{-0.026\pm0.04}$ near the sidewall, and $L_x/H \sim Ra^{0.043\pm0.04}$ and $L_z/H \sim Ra^{-0.0046\pm0.04}$ near the bottom plate.

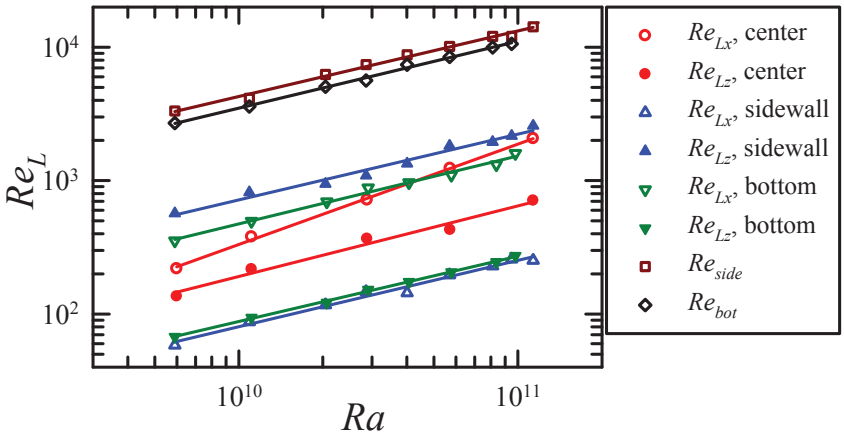

Figure 2. The Ra-dependence of Re_{Lx} and Re_{Lz} measured at cell center (red circles), near the cell sidewall (blue up-triangles), and near the bottom plate (green down-triangles). Re_{side} and Re_{bot} are also plotted for comparison. The lines represent power-law fits to the data.

flow conditions and parameters for each measurement are provided in tables 1, 2, and 3 for the center, sidewall, and bottom-plate measurements, respectively.

3. Results and discussions

3.1. Properties of integral scales

A key response of the RBC system to the imposed Ra is the extent of turbulence, characterized by a Reynolds number. Experimentally, the magnitude of the velocity field at different locations and the circulation frequency of the large-scale circulation are often used to define the system Reynolds number (see, for a recent review, Ahlers *et al.*, 2009). However, the study on the relationship between Ra and the Reynolds number based on the integral length scale, Re_{Li}, defined as

$$Re_{Li} = \frac{\sigma_{Li} L_i}{\nu}, \tag{2}$$

is very limited. Here, $i = x, y$, and z, L_i is the longitudinal integral length scale obtained by integrating the longitudinal autocorrelation function of the i^{th} component of the velocity, and $\sigma_{Li} = \langle |v_i(x+L_i) - v_i(x)|^2 \rangle^{1/2}$ is the RMS value of the longitudinal velocity increment across the scale L_i. In the present study, the technique of spatial multi-point velocity measurements, i.e. the PIV technique, enables us to measure directly L_i and σ_{Li}, and hence Re_{Li}. Figure 1 shows the Ra-dependence of L_x/H and L_z/H at the three different locations. It is seen that L_x/H increases with increasing Ra at the cell center, whereas all other L_x/H and L_z/H are essentially independent of Ra within the error bar. A possible reason for this is that with increasing Ra the sloshing motion of the large-scale circulation (Xi *et al.*, 2009; Zhou *et al.*, 2009) may increase the coherence of the horizontal motion of the fluid at the cell center, resulting in an increases of L_x/H of the flow field. Figure 2 shows in a log-log plot the measured Re_{Lx} and Re_{Lz} vs Ra at the three different locations. The lines are power-law fits to the data, which give

$$\text{At the cell center,} \quad \begin{cases} Re_{Lx} = (9.9 \pm 1.0) \times 10^{-6} Ra^{0.75 \pm 0.05} \\ Re_{Lz} = (9.8 \pm 1.0) \times 10^{-4} Ra^{0.53 \pm 0.05}. \end{cases} \tag{3}$$

$$\text{Near the cell sidewall,} \quad \begin{cases} Re_{Lx} = (8.4 \pm 0.8) \times 10^{-4} Ra^{0.50 \pm 0.04} \\ Re_{Lz} = (8.4 \pm 0.8) \times 10^{-3} Ra^{0.49 \pm 0.04}. \end{cases} \tag{4}$$

$$\text{Near the bottom plate,} \quad \begin{cases} Re_{Lx} = (3.7 \pm 0.4) \times 10^{-3} Ra^{0.51 \pm 0.04} \\ Re_{Lz} = (1.1 \pm 0.1) \times 10^{-3} Ra^{0.49 \pm 0.04}. \end{cases} \tag{5}$$

One sees that all measured Re_{Li} scales as $Ra^{1/2}$ except Re_{Lx} obtained at the cell center, which scales as $Ra^{0.75}$. Such a large scaling exponent between Re_{Lx} and Ra may be due to the increase of L_x/H with increasing Ra. For comparison with the traditional Reynolds number of the large-scale circulation, we also plot in figure 2 the Ra-dependence of Re_{side} and Re_{bot}. Here, $Re_{side} = w_{sm}H/\nu$ and $Re_{bot} = u_{bm}H/\nu$ with w_{sm} being the maximum vertical velocity near the cell sidewall and u_{bm} the maximum horizontal velocity near the bottom plate. The best power-laws to the data give

$$\begin{aligned} Re_{side} &= (0.052 \pm 0.005) Ra^{0.49 \pm 0.04} \\ Re_{bot} &= (0.034 \pm 0.003) Ra^{0.50 \pm 0.04}, \end{aligned} \quad . \tag{6}$$

which share the same scaling exponents as those previously found in cylindrical (Lam *et al.*, 2002) and rectangular (Xia *et al.*, 2003, 2005) cells. It can be seen that except for Re_{Lx} at the cell center, all Re_{Lx} and Re_{Lz} share the same scaling exponents as Re_{side} and Re_{bot} within experimental uncertainty, but Re_{side} and Re_{bot} have a much larger magnitude.

It is usually assumed that velocity increments $\delta_L v$ across the integral length scale L are Gaussian distributed, i.e. $P(\delta_L v) \sim \exp(-\delta_L v^2/2)$. However, such an assumption of Gaussianity has not been verified in the turbulent RBC system. To test this, we measured the global velocity field over an area of 49×49 cm^2 ($\Delta_\ell = 7.76$ mm) in the convection cell using the PIV method and obtained the integral-scale velocity increments at the three locations. Figure 3 shows the PDF of $\delta_L w$ at cell center and near the sidewall and that of $\delta_L u$ near the bottom plate. One finds surprisingly that the measured PDFs exhibit decaying exponential tails at all three locations, rather than Gaussian distribution (dashed curve in the figure). This is different from all known experiments and simulations of isotropic turbulence. To offer a plausible explanation, we note that the turbulent flow in our system is driven by buoyancy in the vertical direction, which is also believed to be the dominant force governing the cascade dynamics above the so-called Bolgiano scale (Lohse & Xia, 2010). In the time domain, it has been found that the Bolgiano timescale

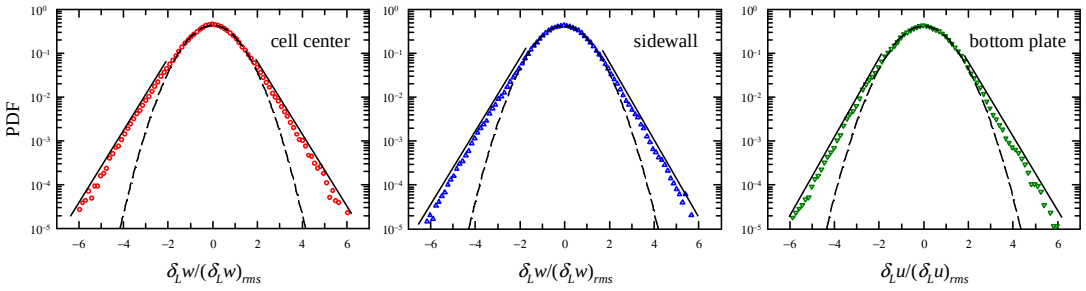

Figure 3. PDFs of the vertical velocity increments $\delta_L w$ at cell center (left) and near the sidewall (center) and that of the horizontal velocity increments $\delta_L u$ near the bottom plate (right) at $Ra = 9.5 \times 10^{10}$ and $Pr = 5.5$. The dashed line is a Gaussian distribution for reference.

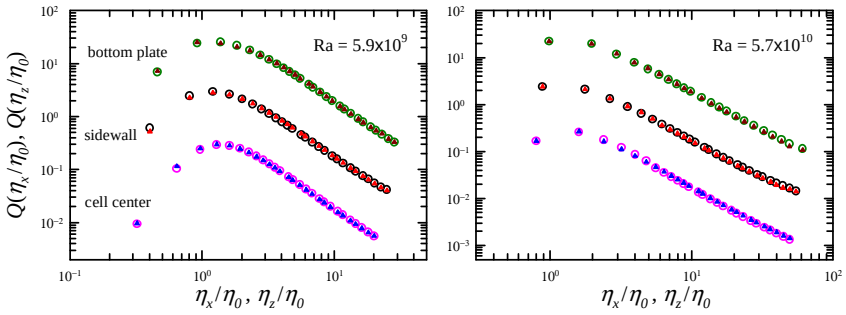

Figure 4. PDFs of the local dissipation scales for the horizontal and vertical velocity components, $Q(\eta_x/\eta_0)$ (open circles) and $Q(\eta_z/\eta_0)$ (solid triangles), measured at different locations and for $Ra = 5.9 \times 10^9$ (a) and 5.7×10^{10} (b). For clarity, results obtained near the sidewall and near the bottom plate are shifted upwards by one and two decades, respectively, with respect to those obtained at cell center.

in turbulent RBC is of order one second (Ching *et al.*, 2004; Zhou & Xia, 2008), which is only a factor of 2 or 3 smaller than the integral timescale. The observed exponential distributions of $\delta_L u$ and $\delta_L w$ may thus come from the buoyancy-induced intermittency, which is then transferred from large to small scales.

3.2. Properties of local dissipation scales

The PDF $Q(\eta)$ is determined from the measured velocity fields in the following way. We first fix a length ℓ that is an integral multiple of the spatial resolution Δ_l, i.e. $\ell = n\Delta_l$. The longitudinal velocity increments across the separation ℓ in both horizontal and vertical directions, $\delta_\ell u$ and $\delta_\ell w$, are then calculated for each velocity vector measured at each discrete time t. If either of the obtained values of $\ell|\delta_\ell u|/\nu$ and $\ell|\delta_\ell w|/\nu$ are between 0.9 and 2 Bailey *et al.* (2009), they contribute to the occurrence of local dissipation at a scale $\ell = \eta$. $Q(\eta)$ is then determined as

$$Q(\eta) = qn(\eta)/N(\eta), \tag{7}$$

where $N(\eta)$ is the total number of calculated velocity increments over a separation η, $n(\eta)$ is the count of events among $N(\eta)$ that satisfy the local balance at scale η, and q is a normalization parameter determined from $\int Q(\eta)d\eta = 1$. In the following, three PDFs are presented. $Q(\eta_x)$ is obtained from the u component only and $Q(\eta_z)$ from the w component. Whereas, $Q(\eta)$ contains contributions from both the horizontal and vertical velocity components.

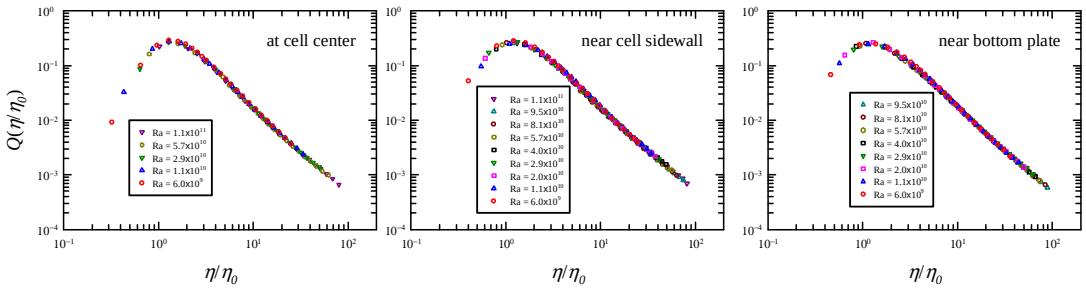

Figure 5. The measured $Q(\eta/\eta_0)$ for various values of Ra.

Figures 4(a) and (b) show log-log plots of $Q(\eta_x/\eta_0)$ (open circles) and $Q(\eta_z/\eta_0)$ (solid triangles) measured at the three locations. As one can see in tables 1, 2, and 3, the scales $\eta_{0x} = L_x \mathrm{Re}_{Lx}^{-0.72}$ and $\eta_{0z} = L_z \mathrm{Re}_{Lz}^{-0.72}$ (Schumacher, 2007) are nearly the same at all locations and for all Ra. Therefore, we use the averaged scale $\eta_0 = (\eta_{0x} + \eta_{0z})/2$ to rescale the results. One sees that at each measuring location the distributions obtained in horizontal and vertical directions coincide excellently with each other within all measured scales, suggesting that the turbulent dynamics of the dissipative range in buoyancy-driven turbulence is isotropic. As the flow is driven by buoyancy in the vertical direction, this result is somewhat unexpected and surprising, especially for data obtained in the plume-dominated regions near the sidewall and near the bottom plate where the turbulent flow is highly anisotropic. The results shown in figure 4 reveal that such buoyancy-induced anisotropy cannot be captured efficiently by $Q(\eta)$ for velocity components along different directions. Hereafter, we will discuss only $Q(\eta)$.

Figure 5 shows $Q(\eta/\eta_0)$ for all values of Ra. The figure appears to show that the shape of $Q(\eta)$ is independent of Ra. However, as we shall see below, predictions of theoretical models, i.e. equations (8) and (9), both show a dependence on Re_L (thus Ra). This is because comparing to the dependence on η, the dependence on Re_L is weak and over the parameter range of our experiment this weak Re_L-dependence cannot be manifested clearly in the measured $Q(\eta)$. With the measured $Q(\eta/\eta_0)$, one can estimate a mean dissipation scale from its first moment. Here, we find that $\langle\eta\rangle = 7.1\eta_0$, $7.7\eta_0$, and $8.1\eta_0$ for distributions obtained at cell center, near the sidewall, and near the bottom plate, respectively. These mean values of η are close to $10\eta_K$, which is located at the lower end of the inertial range (Sun *et al.*, 2006; Zhou *et al.*, 2008). Note that because of the limited resolution our present results could not properly resolve the left tail of $Q(\eta/\eta_0)$ when $Ra \gtrsim 5.7 \times 10^{10}$ [figure 4(b)].

In figure 6, we compare $Q(\eta/\eta_0)$ measured at the three representative locations: at nearly homogeneous and isotropic cell center (circles) and in the plume-dominated regions near the sidewall (up-triangles) and near the bottom plate (down-triangles). It is seen that the three distributions are nearly identical with each other. This suggests that $Q(\eta/\eta_0)$ is insensitive to the large-scale inhomogeneity of turbulent RBC, further indicating the universality of $Q(\eta/\eta_0)$ (for the same type of flow). Nevertheless, one can also see that $Q(\eta/\eta_0)$ measured in the plume-dominated regions exhibit a less-steep left tail than that measured at cell center. An increase of the probabilities at the smallest values of η/η_0 indicates the enhanced velocity gradients at these scales and hence is a manifestation of the increased level of small-scale intermittency. As the Ra-dependence of $Q(\eta/\eta_0)$ is weak, this feature could be attributed to the presence of coherent structures, like plumes, in the near-wall regions. In the figure, numerical and experimental data from homogeneous isotropic box turbulence (Schumacher, 2007) and from turbulent pipe flows (Bailey *et al.*, 2009) are also shown. (The two data were both taken from figure 4 of Bailey *et al.* (2009) using a data capturing software.) Good agreements can be seen in the right tails, whereas,

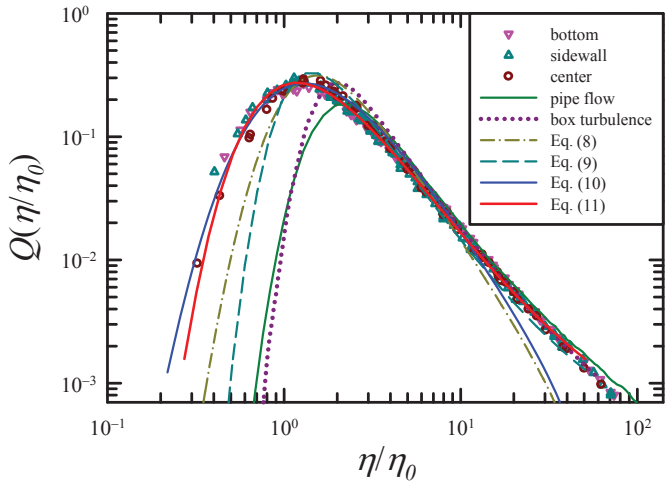

Figure 6. Comparison among $Q(\eta/\eta_0)$ measured at the three representative locations in the cell for all values of Ra, the experimental result from turbulent pipe flow Bailey *et al.* (2009), the numerical result for box turbulence Schumacher (2007), and the theoretical distributions according to Eqs. (8), (9), (10), and (11) obtained with $\mathrm{Re}_L = 217$ (the Reynolds number obtained at cell center for $\mathrm{Ra} = 1.1 \times 10^{10}$).

for the left tail at small η, our results exhibit much higher probabilities. This suggests a much higher level of small-scale intermittency possessed by our thermal turbulence in comparison to those of box turbulence and turbulent pipe flows, although the nominal Reynolds numbers for our flow are comparable or even smaller than the latter two cases. This may be understood by the presence of thermal plumes, which have a characteristic dimension of thermal boundary layer that is smaller than η_K.

The theoretical $Q(\eta)$ can be derived in several ways. Using the Mellin transform of structure functions, Yakhot (2006) showed that

$$Q(\eta) = 2/\{\pi\eta[b\log(L/\eta)]^{1/2}\}\int_0^\infty dx\exp[-x^2 - \frac{\{\log[\frac{\sqrt{2}x\mathrm{Re}_L}{c}(\frac{\eta}{L})^{a+1}]\}^2}{4b\log(L/\eta)}], \quad (8)$$

within the range $0 < \eta < L$, where $a = 0.383$, $b = 0.0166$, and $c = O(1)$ is a fitting parameter (Schumacher, 2007; Bailey *et al.*, 2009). Based on the multifractal formalism and using the Batchelor parametrization, Biferale (2008) obtained

$$Q(\tilde{\eta}) = \int dh A^{4-h-D(h)}\mathrm{Re}_L^{[3h+3D(h)-10]/4}\tilde{\eta}^{1-h-D(h)}\exp[-0.5A^{2(1-h)}\mathrm{Re}_L^{(3h-1)/2}\tilde{\eta}^{-2(1+h)}], \quad (9)$$

where $A = O(1)$ is a fitting parameter, h is the local scaling (or Hölder) exponent, $D(h)$ is the multifractal dimension spectrum, and $\tilde{\eta} = \eta/\eta_K$ with $\eta_K = L\mathrm{Re}_L^{-3/4}$.[1] In figure 6 we compare directly the theoretical $Q(\eta/\eta_0)$ according to equations (8) and (9) with our measured results.[2]

[1] In the evaluations of euqations (9) and (11), the log-Poisson spectrum (She & Leveque, 1994), $D(h) = 3(h - \frac{1}{9})/\log(\frac{2}{3})[\log(3(\frac{1}{9} - h)/2\log(\frac{2}{3})) - 1] + 1$, was chosen and the integral was evaluated within the range $h_{min} < h \leq h_{max}$, where $h_{min} = \frac{1}{9}$ and $h_{max} = 0.38$ is obtained such that $D(h)$ reaches its maximum value of 3 at $h = h_{max}$.

[2] Note that both the parameters A and c essentially control the peak position of the theoretically-predicted $Q(\eta)$,

Here we see that our measured $Q(\eta)$ have much higher values at small η than both theoretical predictions.

To understand such a discrepancy, we note that both theoretical approaches (Yakhot, 2006; Biferale, 2008) used the assumption that velocity increments $\delta_L v$ across the integral length scale L are Gaussian distributed, i.e. $P(\delta_L v) \sim \exp(-\delta_L v^2/2)$. Specifically, the left tail of $Q(\eta)$ is dominated by contributions from the stretched exponential in equation (9), which stems from the Gaussian-distributed integral-length-scale velocity. However, in the present system, figure 3 has shown that the measured PDFs of $\delta_L v$ exhibit decaying exponential tails at all three locations, rather than Gaussian distribution. Motivated by this, we now modify the two models proposed by Yakhot and Biferale, respectively. Following the same derivations as in references Yakhot (2006) and Biferale (2008), but instead using the exponential distribution $P(\delta_L v) \sim \exp(-|\delta_L v|)$ for the integral-length-scale velocity increments, we obtain, respectively,

$$Q(\eta) = 1/\{\eta[b\pi \log(L/\eta)]^{1/2}\} \int_0^\infty dx \exp[-x - \frac{\{\log[\frac{x\mathrm{Re}_L}{c}(\frac{\eta}{L})^{a+1}]\}^2}{4b\log(L/\eta)}], \tag{10}$$

and

$$Q(\tilde{\eta}) = \int dh A^{4-h-D(h)} \mathrm{Re}_L^{[3h+3D(h)-10]/4} \tilde{\eta}^{1-h-D(h)} \exp[-A^{(1-h)} \mathrm{Re}_L^{(3h-1)/4} \tilde{\eta}^{-(1+h)}]. \tag{11}$$

Figure 6 shows direct comparison of $Q(\eta/\eta_0)$ according to equations (10) (blue solid line) and (11) (red solid line) and our measured results. The excellent agreement between the experimental and theoretical results for nearly all measured η can be seen, except for equation (10) at large η. This excellent agreement with both predictions suggests that the models developed for isotropic and homogeneous turbulence can also be applied to buoyancy-driven turbulence, like turbulent RBC. It is in this sense that our results reveal that the local dissipation scale dynamics is universal, whereas the exact shape of the local dissipation scale PDF (specifically, its left part) obviously depends on the integral-scale velocity boundary condition.

4. Acknowledgments

This work was supported by the Research Grants Council of Hong Kong SAR (No. CUHK403807 and 404409). Q. Z. thanks the support of Natural Science Foundation of China (No. 11002085), "Pu Jiang" project of Shanghai (No. 10PJ1404000), "Chen Guang" Project of Shanghai (No. 09CG41), and Shanghai Program for Innovative Research Team in Universities.

References

Ahlers, G., Grossmann, S. & Lohse, D. 2009 Heat transfer and large scale dynamics in turbulent Rayleigh-Bénard convection. *Rev. Mod. Phys.* **81**, 503–537.

Bailey, S. C. C., Hultmark, M., Schumacher, J., Yakhot, V. & Smits, A. J. 2009 Measurement of local dissipation scales in turbulent pipe flow. *Phys. Rev. Lett.* **103**, 014502.

Biferale, L. 2008 A note on the fluctuation of dissipative scale in turbulence. *Phys. Fluids* **20**, 031703.

in the two models respectively. Here, we choose $A = 4$ and $c = 2$ to fit our experimental results. If different values of A and c were chosen, the predictions of the two models would fit the data of turbulent pipe flow and box turbulence much better than they appear in figure 6 (see, e.g., Schumacher, 2007; Biferale, 2008; Bailey *et al.*, 2009). These fittings are not shown here to avoid overcrowding the figure and also because the purpose here is to compare the theoretical predictions with our measured data.

Ching, E. S. C., Chui, K. W., Shang, X.-D., Qiu, X.-L., Tong, P. & Xia, K.-Q. 2004 Velocity and temperature cross-scaling in turbulent thermal convection. *J. Turbulence* **5**, 27.

Frisch, U. 1995 *Turbulence: the legacy of A. N. Kolmogorov*. Cambridge Univ. Press.

Ishihara, T., Gotoh, T. & Kaneda, Y. 2009 Study of high-Reynolds number isotropic turbulence by direct numerical simulation. *Annu. Rev. Fluid Mech.* **41**, 165–180.

Kolmogorov, A. N. 1941 The local structure of turbulence in the incompressible viscous fluid for very large Reynolds numbers. *Dokl. Akad. Nauk. SSSR* **30**, 301–305.

Lam, S., Shang, X.-D., Zhou, S.-Q. & Xia, K.-Q. 2002 Prandtl number dependence of the viscous boundary layer and the Reynolds numbers in Rayleigh-Bénard convection. *Phys. Rev. E* **65**, 066306.

Lohse, D. & Xia, K.-Q. 2010 Small-scale properties of turbulent Rayleigh-Bénard convection. *Annu. Rev. Fluid Mech.* **42**, 335–364.

Paladin, G. & Vulpiani, A. 1987 Degrees of freedom of turbulence. *Phys. Rev. A* **35**, 1971–1973.

Schumacher, J. 2007 Sub-Kolmogorov-scale fluctuations in fluid turbulence. *Europhys. Lett.* **80**, 54001.

She, Z.-S. & Leveque, E. 1994 Universal scaling laws in fully developed turbulence. *Phys. Rev. Lett.* **72**, 336–339.

Sreenivasan, K. R. & Antonia, R. A. 1997 The phenomenology of small-scale turbulence. *Annu. Rev. Fluid Mech.* **29**, 435–472.

Sun, C., Ren, L.-Y., Song, H. & Xia, K.-Q. 2005 Heat transport by turbulent Rayleigh-Bénard convection in 1 m diameter cylindrical cells of widely varying aspect ratio. *J. Fluid Mech.* **542**, 165–174.

Sun, C., Zhou, Q. & Xia, K.-Q. 2006 Cascades of velocity and temperature fluctuations in buoyancy-driven thermal turbulence. *Phys. Rev. Lett.* **97**, 144504.

Xi, H.-D., Zhou, S.-Q., Zhou, Q., Chan, T.-S. & Xia, K.-Q. 2009 Origin of the temperature oscillation in turbulent thermal convection. *Phys. Rev. Lett.* **102**, 044503.

Xia, K.-Q., Sun, C. & Zhou, S.-Q. 2003 Particle image velocimetry measurement of the velocity field in turbulent thermal convection. *Phys. Rev. E* **68**, 066303.

Xia, K.-Q., Zhou, S.-Q. & Sun, C. 2005 Statistics and scaling of the velocity field in turbulent thermal convection. In *Progress in Turbulence* (ed. J. Peinke, A. Kittel, S. Barth & M. Oberlack), pp. 163–170. Springer.

Yakhot, V. 2006 Probability densities in strong turbulence. *Physica D* **215**, 166–174.

Yakhot, V. 2008 Dissipation-scale fluctuations and mixing transition in turbulent flows. *J. Fluid Mech.* **606**, 325–337.

Zhou, Q., Li, C.-M., Lu, Z.-M. & Liu, Y.-L. 2011 Experimental investigation of longitudinal space-time correlations of the velocity field in turbulent Rayleigh-Bénard convection. *J. Fluid Mech.* **in press**.

Zhou, Q., Sun, C. & Xia, K.-Q. 2008 Experimental investigation of homogeneity, isotropy and circulation of the velocity field in buoyancy-driven turbulence. *J. Fluid Mech.* **598**, 361–372.

Zhou, Q., Xi, H.-D., Zhou, S.-Q., Sun, C. & Xia, K.-Q. 2009 Oscillations of the large-scale circulation in turbulent Rayleigh-Bénard convection: the sloshing mode and its relationship with the torsional mode. *J. Fluid Mech.* **630**, 367–390.

Zhou, Q. & Xia, K.-Q. 2008 Comparative experimental study of local mixing of active and passive scalars in turbulent thermal convection. *Phys. Rev. E* **77**, 056312.

Zhou, Q. & Xia, K.-Q. 2010 Universality of local dissipation scales in buoyancy-driven turbulence. *Phys. Rev. Lett.* **104**, 124301.